Infrared emission from holmium doped gallium lanthanum sulphide glass

T. Schweizer, B.N. Samson, J.R. Hector, W.S. Brocklesby, D.W. Hewak, and D.N. Payne

Optoelectronics Research Centre, University of Southampton, Southampton, SO17 1BJ, UK

Tel.: +44-1703-593141

Fax: +44-1703-593142

email: ts@orc.soton.ac.uk

Abstract

Infrared emission at 1.2, 1.25, 1.67, 2.0, 2.2, 2.9, 3.9, and 4.9 μm is measured in holmium (Ho^{3+}) doped gallium lanthanum sulphide (GLS) glass. Branching ratios, radiative quantum efficiencies, and emission cross sections are calculated from lifetime, absorption, and emission measurements using Judd-Ofelt analysis and the Füchtbauer-Ladenburg equation. The fluorescence band at 3.9 μm coincides with an atmospheric transmission window and the fluorescence band at 4.9 μm overlaps with the fundamental absorption of carbon monoxide, making the glass a potential fibre laser source for remote sensing and gas sensing applications. This is the first time this latter transition has been reported in any holmium doped host.

PACS codes: 42.70.C, 42.72.A, 42.70.H

Keywords: chalcogenide glass, holmium, infrared, spectroscopy

1. Introduction

Most gas molecules have strong fundamental absorption bands in the mid-infrared wavelength region (3-5 μm). These specific "fingerprints" can be used to identify gas species, and the strength of the absorption over a certain path length includes information about the concentration of a particular species in a gas mixture. Mid-infrared light sources would therefore find application in atmospheric sensing of environmentally important gases such as methane, nitrogen dioxide, carbon dioxide, and carbon monoxide, and in on-line monitoring of exhaust gas pollution by industrial plants, vehicles, and jet engines. Other possible applications include optical radar, e.g. collision avoiding radar, ammonia and water vapour sensing in agriculture, medical diagnostics, molecular spectroscopy, point-to-point atmospheric communication, remote control, etc. The most promising example of the group of mid-infrared emitting light sources, which includes thermal emitters, optical parametric oscillators, and difference frequency generation, are the semiconductor light emitting diodes (LED) and laser diodes. A good overview about the application of laser diodes for monitoring gaseous pollutants can be found in Ref. [1].

It is less well known that rare-earth doped materials are also capable of emitting mid-infrared radiation. Transitions between closely spaced electronic energy levels (2000-3300 cm^{-1}) of trivalent rare-earth ions emit radiation in the 3-5 μm wavelength range if the transition probability of competing non-radiative transitions is kept as low as possible by choosing a host material with a low phonon energy. The rare-earth laser with the longest emission wavelength reported to date operates in a pulsed mode at room temperature at a wavelength of 7.2 μm in a praseodymium (Pr^{3+}) doped $LaCl_3$ crystal [2]. The only rare-earth doped laser operating *continuous wave at room temperature* at a wavelength longer than 3 μm is the 3.5 μm erbium (Er^{3+})

doped fluorozirconate (ZBLAN) fibre laser which benefits from the advantages of the fibre geometry [3]. The fibre geometry offers high gain due to the long interaction length of pump and laser modes, small pump powers due to the high intensities in the fibre core, favourable thermal conditions due to the good heat dissipation, and the possibility to exploit weak rare-earth absorption bands due to the long optical path in the fibre. The longest emission wavelength of a fibre laser was obtained in a holmium (Ho^{3+}) doped ZBLAN fibre [4]. This laser operates continuous wave at a wavelength of 3.9 μm but needs cryogenic cooling to reduce the competing non-radiative decay processes which depopulate the upper laser level. As an alternative to cooling the multiphonon decay rate can be reduced by choosing a host material with an even lower phonon energy than fluorozirconate glass (~ 580 cm^{-1}). Chalcogenide glasses, non-oxide glasses based on sulphur, selenium, or tellurium, have lower phonon energies (~ 300 - 400 cm^{-1}), a good infrared transparency, and can be fabricated into fibre form [5,6]. Mid-infrared fluorescence has previously been reported from Pr^{3+}, Dy^{3+} (dysprosium), and Er^{3+} doped chalcogenide glasses [7-9].

In this paper we present spectroscopic data of infrared emission bands from Ho^{3+} doped gallium lanthanum sulphide (GLS) glass. We chose GLS from the group of chalcogenide glasses because it combines several desirable properties. The glass is nontoxic (no As, Se, Te, etc.), chemically stable (non-hygroscopic) and has a high glass transition temperature (561°C compared to 153°C for As_2S_3 and 47°C for As_5Se_{95}) making the glass more resistant to environmental effects and thermal damage by high power pump laser sources. Other advantages include the good transparency in the visible and near-infrared pump wavelength range and the mid-infrared laser wavelength range, along with a high rare-earth solubility due to the presence of lanthanum in the glass matrix. Furthermore, GLS can be melted in large

glass ingots and, most importantly, can be pulled into fibre form using the rod-in-tube technique [10].

Ho^{3+} doped GLS glasses have first been reported 20 years ago by Reisfeld and co-workers with emphasis on visible and near-infrared emission [11-13]. Since then the qualities of the glasses has improved considerably, in particular due to the reduction of lanthanum oxide and hydroxyl impurities.

In the present work Ho^{3+} doped glasses have been characterised by absorption, fluorescence, and lifetime spectroscopy. The radiative properties of the infrared transitions such as radiative rates, branching ratios, radiative lifetimes, and emission cross sections have been obtained from Judd-Ofelt calculations and the Füchtbauer-Ladenburg equation. Infrared emission bands have been observed at 1.2, 1.25, 1.67, 2.0, 2.2, 2.9, 3.9, and 4.9 μm, some of which have not been reported in glass or other rare-earth host materials before.

2. Experiments

We melted a series of GLS glasses with the molar ratio $70Ga_2S_3$:$30La_2S_3$ and doped them with Ho^{3+} by replacing La_2S_3 with the required amount of Ho_2S_3. Glasses were doped with 0.05 mol. % Ho_2S_3 ($n_{Ho} = 8.9 \times 10^{18}$ ions/cm^3), 0.2 mol. % Ho_2S_3, and 1.5 mol. % Ho_2S_3. These samples will be referred to simply by Ho(0.05%):GLS, etc. The glasses were cut and polished on three sides for absorption, fluorescence, and lifetime measurements. Absorption spectra were measured from 0.45 μm to 2.25 μm with a Perkin-Elmer Lambda 9 spectrophotometer. Samples were excited with a tuneable Ti:sapphire laser at 0.76 μm and 0.9 μm, and a 2 μm diode pumped Tm:YAG laser for fluorescence and lifetime measurements. Fluorescence spectra were recorded with a computer driven monochromator and an InGaAs detector (1.1 -

1.4 μm) or liquid nitrogen cooled InSb detector (1.5 - 5.45 μm). Fluorescence decay curves were measured with a photomultiplier (0.76 μm), with an InGaAs detector (0.9 μm), and a liquid nitrogen cooled InSb detector (2.0 μm) using an acousto-optic modulator or a chopper to modulate the pump beam and a monochromator or a suitable set of filters for wavelengths discrimination. The decay curves were averaged using a photon counting device (Stanford Model SR430 Multi-Channel Scaler) for the photomultiplier and a TEK2232 digital storage oscilloscope for the InGaAs and InSb detectors and transferred to a personal computer for the fitting procedure. All measurements were performed at room temperature.

3. Results and Discussion

Fig. 1 shows the ground state absorption bands from the $^5I_8$ to the seven lowest energy levels for a Ho(1.5%):GLS glass and Fig. 2 a schematic energy level diagram. The electronic absorption edge of the host glass starts at about 0.5 μm and obscures the higher energy levels of the rare-earth ($^5F_3$, $^5F_2$, etc.). The closely spaced $^5S_2$,$^5F_4$ levels have been treated as one level for the Judd-Ofelt calculations. The infrared multiphonon absorption edge of the glass starts at about 8 μm (not shown). The location and spectral shape of the Ho^{3+} absorption bands are similar to other glasses. The strength of the absorption bands, however, is larger due to the large covalency and large refractive index of the glass bonds [14].

We excited the Ho^{3+} ions for fluorescence measurements into the 0.76 μm band populating the $^5I_4$ level and subsequently the $^5I_5$, $^5I_6$, and $^5I_7$ levels via radiative and non-radiative transitions (Fig. 2). Although the strength of this absorption band is particularly weak (inset in Fig. 1) it was chosen for its convenient pump wavelength. Pumping at 0.76 μm not only populates the lower but also some higher energy levels

leading to green and red upconversion emission from the $^5F_4$,$^5S_2$ levels and the $^5F_5$ level. For lifetime measurements the $^5I_4$, $^5I_5$, and $^5I_7$ levels were excited resonantly at 0.76 μm and 0.9 μm and at 2.0 μm, respectively, in order to avoid distortion of the fluorescence decay times of these levels caused by population from higher energy levels.

The identification and characterisation of potential laser transitions in Ho^{3+} doped GLS glass requires an understanding of the spectroscopic properties of this material. The radiative properties of the fluorescent Ho^{3+} transitions can be obtained from Judd-Ofelt calculations [15,16]. The absorption spectra of Ho^{3+} doped GLS glasses were used to calculate the Judd-Ofelt parameters which in turn allow the calculation of the radiative rates, lifetimes, and branching ratios of the fluorescent transitions. All six absorption bands shown in Fig. 1 were used in the fitting after subtracting the magnetic dipole contribution of the $^5I_8 \rightarrow {}^5I_7$ transition. The electric and magnetic dipole contributions, A_{ed} and A_{md}, of the radiative transition rate $A = A_{ed} + A_{md}$ were calculated from the equations given in ref. [17] and are listed in Table 1. The branching ratios $\beta = A / A_{total}$ and the radiative lifetimes $\tau_r = 1 / A_{total}$ were derived from the radiative rates. Comparison of τ_r with the measured lifetimes τ_m gives the quantum efficiencies $\eta = \beta \times (\tau_m / \tau_r)$. The measured lifetimes in Table 1 were obtained from the sample with the low Ho^{3+} concentration of 0.05 mol% but are very similar to the lifetimes measured in glasses with higher concentrations of 0.2 and 1.5 mol% indicating a very low probability of lifetime quenching by ion-ion interactions. The lifetime of the $^5I_6$ level could not be measured due to the lack of a 1.2 μm pump source but is expected to be very close to the calculated radiative lifetime of 1.65 ms because the rate of multiphonon decay should be negligible. Unlike β, which is only

weakly dependent on the host material, A (and therefore τ_r) and τ_m (and therefore η) show a much stronger dependence.

The above parameters have been compared among various chalcogenide glasses, a fluorozirconate glass (ZBLAN) and a silicate glass for one specific transition. The Judd-Ofelt parameters for Ho^{3+} along with the radiative rates, the measured lifetimes, the quantum efficiencies, and the emission cross sections of the $^5I_7 \rightarrow {}^5I_8$ transition (2.0 μm) are listed in Table 2. The Ω_2 and Ω_4 values we obtained do not agree with the values reported in the early 80's for a GLS glass with a slightly different composition (75:25 compared to 70:30) but the Ω_2 value is in line with the values published for the other two chalcogenide glasses [13,18]. The Judd-Ofelt parameter Ω_2, the radiative rates A, and the emission cross sections σ_{em} are higher in chalcogenide glasses compared to fluoride (ZBLAN) and silicate glasses, which is a result of the large covalency of the glass bonds [14].

The measured lifetimes reflect the variations in both the radiative rates (mostly via changes in the refractive index of the glass) and the multiphonon decay rates (via changes in the phonon energy) in these hosts. The lifetime is the longest in the fluoride glass largely due to the low radiative rate (ionic, low refractive index of 1.5) and also to the low non-radiative rate (small phonon energy of ~ 580 cm^{-1}). It is shorter in the GLS glass due to the higher radiative rates (strongly covalent, high refractive index of 2.4), but shortest in the silicate glass due to the high non-radiative rate (large phonon energy of ~ 1160 cm^{-1}). Hence the low quantum efficiency of the $^5I_7$ level in the silicate glass. For the chalcogenide and the fluoride glass the 2 μm transition is almost purely radiative, so the quantum efficiencies are nearly 100%. However, this does not apply to energy levels with an even smaller energy gap to the next lower lying level, such as the $^5I_4$, $^5I_5$, and the $^5I_6$ levels. For these levels non-

radiative decay becomes important in fluoride glasses decreasing the lifetimes and the fluorescence intensities. Emission from the $^5I_4$ level has not been reported in fluoride glasses but could be measured in GLS glass in this work.

The emission cross sections (Table 1.) were calculated using the Füchtbauer-Ladenburg equation as given in [21]:

$$\sigma_{em}(\lambda) = \frac{A\lambda^5 I(\lambda)}{8\pi n^2 c \int \lambda I(\lambda) d\lambda} \quad (1)$$

$I(\lambda)$ is the measured intensity spectrum of the fluorescence, n is the refractive index.

We also applied the theory of McCumber after Miniscalco and Quimby [22] to calculate the emission cross sections of the 2 μm ground state transitions from the measured absorption spectrum. The value of 0.95×10^{-20} cm^2 from the McCumber method confirms the value of 1.08×10^{-20} cm^2 from the Füchtbauer-Ladenburg equation and gives us some confidence in the accuracy of the cross sections in Table 1.

We can compare the prospective emission wavelengths of Ho:GLS fibre lasers with reported work on Ho:silica and Ho:fluoride fibre lasers. In a silica fibre, laser operation on the 2 μm ground state transition has been reported despite the low radiative quantum efficiency, estimated to be about 1.5% [23]. The low quantum efficiency increased the threshold pump power. The higher energy levels $^5I_6$, $^5I_5$, and $^5I_4$ have even smaller energy gaps to the next lower lying levels, increasing the multiphonon decay rates and quenching fluorescence from these levels in silica glass (see Fig. 2).

In a fluoride glass fibre, reduced multiphonon rates increase the radiative quantum efficiency for the $^5I_6$ level to about 60%, making room temperature continuous wave

laser operation at 1.2 and 2.9 μm possible [19,24]. However, multiphonon processes from the $^5I_5$ level are so strong that superfluorescence and laser operation at 3.9 μm require cryogenic cooling to reduce the non-radiative decay rate [4,25]. Emission from the $^5I_4$ level with an even smaller energy gap is completely quenched.

In GLS glass, the lower phonon energy leads to emission from all four ^5I_J levels (J=4,5,6,7). Fig. 3.a shows the 2 μm emission from the first excited state $^5I_7$ under continuous wave pumping at 0.76 μm. The 2 μm band overlaps with the 2.2 μm emission from the $^5I_4$ pump level which is not obvious under continuous wave pumping. The strength of the 2 μm transition is much larger than the strength of the 2.2 μm transition due to the higher branching ratio and the higher quantum efficiency (Table 1). Modulating the pump laser at a frequency of 400 Hz decreases the intensity of the 2 μm emission relative to the intensity of the 2.2 μm emission (Fig. 3.b). The $^5I_4$ level is excited directly and instantaneously whereas the $^5I_7$ level is mainly populated by slow radiative decay from the higher levels which cannot follow the fast pump modulation (Fig. 2). The 2.2 μm emission is unique to a host material with a low phonon energy and is not observed in silica and fluoride glasses. The 2.0 μm fluorescence, however, has been measured in other chalcogenide glasses before [18,26].

Near-infrared emission from the $^5I_6$, $^5I_5$, and $^5I_4$ levels is shown in Fig. 4.a and b. While the 1.2 μm and 1.67 μm transitions can also be observed in fluoride glasses, though with lower efficiencies, the 1.25 μm emission is unique to chalcogenide glasses. The 1.67 μm emission coincides exactly with the overtone of the 3.35 μm CH_4 absorption band and is of interest for gas sensing [27].

Fig. 5 shows the emission spectra of three mid-infrared transitions at 2.9, 3.9, and 4.9 μm. The 2.9 μm transition has the highest fluorescence intensity followed by the

3.9 μm and 4.9 μm transitions as expected from the values of the radiative rates and quantum efficiencies (Table 1). Even the 4.9 μm transition still has a quantum efficiency of 1% at room temperature which can be seen as a lower limit for a viable laser transition. However, we note that a lower phonon energy chalcogenide glass could have up to 10% quantum effiency, limited by the branching ratio. While the 2.9 μm emission has been measured before in chalcogenide glasses [18] the 3.9 μm and the 4.9 μm bands have been identified in a chalcogenide glass for the first time in this work. To our knowledge, the 4.9 μm emission has not been reported in any host before.

The 2.9 μm emission band overlaps with the absorption of water and may prove useful for medical applications. The 3.9 μm emission coincides with the attenuation minimum of an atmospheric window making a fibre laser at this wavelength interesting for applications that require a low atmospheric attenuation. The 4.9 μm emission bands overlaps with the absorption bands of CO and OCS gas and could find application as a gas sensor [27].

4. Conclusion

In conclusion, we have presented spectroscopic data of Ho^{3+} doped GLS glasses with respect to their suitability for mid-infrared laser devices. A quantitative analysis using Judd-Ofelt calculations, the Füchtbauer-Ladenburg equation, and the modified McCumber theory along with absorption, fluorescence, and lifetime measurements has delivered important laser parameters such as absorption coefficients, emission cross sections, laser level lifetimes, and quantum efficiencies. The quantum efficiencies and cross sections for mid-infrared transitions are higher than in common silicate and fluoride glasses opening the potential for mid-infrared fibre lasers with

higher efficiencies and longer emission wavelengths. The quantum efficiencies and emission cross sections of the 2.0 μm transition, for example, are 97% and 1.08×10^{-20} cm^2 in GLS glass compared to 2% and 0.70×10^{-20} cm^2 for a typical silicate glass. The fluorescence bands at 2.9, 3.9, and 4.9 μm observed in GLS glass are quenched by non-radiative decay in silicate glasses. The 4.9 μm transition which was reported for the first time still has a quantum efficiency of 1%.

The GLS glass is a promising host material for mid-infrared fibre lasers because it is one of the few chalcogenide glasses that has been pulled into fibre form successfully [10] and is the only rare-earth doped chalcogenide fibre with demonstrated laser action to date [28].

Acknowledgements

This work was supported by the UK EPSRC/DTI LINK programme (LONGWAVE). Chalcogenide powders were supplied by Merck Ltd., Poole, UK, and samples were polished by Crystran Ltd., Poole, UK. Thanks to R.A. Hayward for providing the 2 μm Tm:YAG laser source.

References

[1] Infrared Phys. Technol. **37** (1996) whole issue, Proceedings of the 4th International symposium on monitoring of gaseous pollutants by tunable diode lasers, 19-20 October 1994, Freiburg, Germany, ed. R. Grisar, M. Tacke, H. Böttner

[2] S.R. Bowman, L.B. Shaw, B.J. Feldman, and J. Ganem, IEEE J. Quantum Electron. **32** (1996) 646

[3] H. Többen, Electron. Lett. **28** (1992) 1361

[4] J. Schneider, C. Carbonnier, and U.B. Unrau, Appl. Optics **36** (1997) 8595

[5] P.N. Kumta and S.H. Risbud, J. Mater. Sci. **29** (1994) 1135

[6] H. Suto, Infrared Phys. Technol. **38** (1997) 93

[7] L.B. Shaw, B.B. Harbison, B. Cole, J.S. Sanghera, and I.D. Aggarwal, Optics Express **1** (1997) 87

[8] J. Heo and Y.B. Shin, J. Non-Cryst. Solids **196** (1996) 162

[9] T. Schweizer, D.W. Hewak, B.N. Samson, and D.N. Payne, J. Lumin. **72-74** (1997) 419

[10] D.W. Hewak, R.C. Moore, T. Schweizer, J. Wang, B. Samson, W.S. Brocklesby, D.N. Payne, and E.J. Tarbox, Electron. Lett. **32**, (1996) 384

[11] R. Reisfeld, A. Bornstein, J. Flahaut, M. Guittard, and A.M. Loireau-Lozac'h, Chem. Phys. Lett. **47** (1977) 408

[12] R. Reisfeld, A. Bornstein, J. Bodenheimer, and J. Flahaut, J. Lumin. **18/19** (1979) 253

[13] R. Reisfeld, Ann. Chim. Fr. **7** (1982) 147

[14] C. K. Jørgensen and R. Reisfeld, J. Less-Common Metals **93** (1983) 107

[15] B.R. Judd, Phys. Rev. **127** (1962) 750

[16] G.S. Ofelt, J. Chem. Phys. **37** (1962) 511

[17] M.J. Weber, Phys. Rev. **157** (1966) 262

[18] Y.B. Shin, J.N. Jang, and J. Heo, Opt. Quant. Electron. **27** (1995) 379

[19] L. Wetenkamp, G.F. West, and H. Többen, J. Non-Cryst. Solids **140** (1992) 35

[20] B. Peng and T. Izumitani, Opt. Mater. **4** (1995) 797

[21] B.F. Aull and H.P. Jensen, IEEE J. Quantum Elect. **QE-18** (1982) 925

[22] W.J. Miniscalco and R.S. Quimby, Opt. Lett. **16** (1991) 258

[23] D.C. Hanna, P.M. Percival, R.G. Smart, J.E. Townsend, and A.C. Tropper, Electron. Lett. **25** (1989) 593

[24] L. Wetenkamp, Electron. Lett. **26** (1990) 883

[25] J. Schneider, Int. J. Infrared Millimeter Waves **16** (1995) 75

[26] Y.S. Kim, W.Y. Cho, Y.B. Shin, and J. Heo, J. Non-Cryst. Solids **203** (1996) 176

[27] P. Werle, Infrared Phys. Technol. **37** (1996) 59

[28] T Schweizer, B.N. Samson, R.C. Moore, D.W. Hewak, and D.N. Payne, Electron. Lett. **33**, (1997) 414

Figure captions

Figure 1 Absorption spectrum of 1.5 mol% Ho_2S_3 doped GLS glass. The inset shows the pump absorption band at 0.76 μm.

Figure 2 Energy level diagram and fluorescent transitions of Ho^{3+}

Figure 3 Overlapping emission at 2.0 and 2.2 μm from the $^5I_7$ and the $^5I_4$ levels in Ho(1.5%):GLS pumped at 0.76 μm

a) continuous wave pump laser

b) pump laser chopped at 400 Hz

Figure 4 Near-infrared emission a) from the $^5I_4$ and $^5I_6$ levels, and b) from the $^5I_5$ level in Ho(1.5%)GLS pumped at 0.76 μm

Figure 5 Mid-infrared emission a) from the $^5I_6$ level, b) from the $^5I_5$ level, and c) from the $^5I_4$ level in Ho(1.5%)GLS pumped at 0.76 μm

Tables

Table 1 Radiative properties and emission cross sections of infrared transitions in Ho^{3+} doped GLS glass

Transition	λ (μm)	A_{ed} (s^{-1})	A_{md} (s^{-1})	β (%)	τ_r (ms)	τ_m (ms)	η (%)	$\sigma_{em,FL}$ ($10^{-20}cm^2$)
$^5I_7 \rightarrow {}^5I_8$	2.00	228	95	100	3.10	3.0	97	1.08
$^5I_6 \rightarrow {}^5I_8$	1.19	489		81	1.65			
$\rightarrow {}^5I_7$	2.86	73	44	19				2.22
$^5I_5 \rightarrow {}^5I_8$	0.90	212		42	2.00	1.7	36	
$\rightarrow {}^5I_7$	1.67	239		48			41	0.71
$\rightarrow {}^5I_6$	3.90	28	20	10			9	2.29
$^5I_4 \rightarrow {}^5I_8$	0.76	24		8	3.58	0.5	1	
$\rightarrow {}^5I_7$	1.25	114		41			6	
$\rightarrow {}^5I_6$	2.19	114		41			6	
$\rightarrow {}^5I_5$	4.92	19	8	10			1	1.27

Table 2 Judd-Ofelt parameters, radiative emission probabilities and emission cross sections for the $^5I_7 \rightarrow {}^5I_8$ transition (2.0 μm), and measured lifetimes of the $^5I_7$ level for different Ho^{3+} doped glasses

Glass (Ho^{3+} conc.)	Ω_2 ($10^{20}cm^2$)	Ω_4 ($10^{20}cm^2$)	Ω_6 ($10^{20}cm^2$)	A (s^{-1})	τ_m (ms)	η (%)	σ_{em} ($10^{-20}cm^2$)
GLS (1.5%)	6.9	5.5	1.07	323	3.1	97	1.08
GLS (75:25) [13]	2.31	2.81	1.08				
$3Al_2S_3$:$1La_2S_3$ [13]	8.09	3.85	1.40				
$Ge_{30}As_{10}S_{60}$ [18]	6.98	2.53	0.78	177			
ZBLAN [19]	2.30	2.30	1.71	79	12.01	95	0.56
Silicate (2%) [20]	3.60	3.01	0.61	61.65	0.32	2	0.70

Figure 1

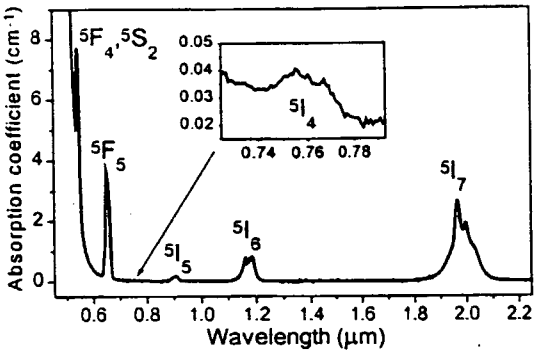
Absorption coefficient (cm-1)
Wavelength (μm)
5F4,5S2
5F5
5I5
5I6
5I7
5I4
0.05
0.04
0.03
0.02
0.74 0.76 0.78
0 2 4 6 8
0.6 0.8 1.0 1.2 1.4 1.6 1.8 2.0 2.2

Figure 2

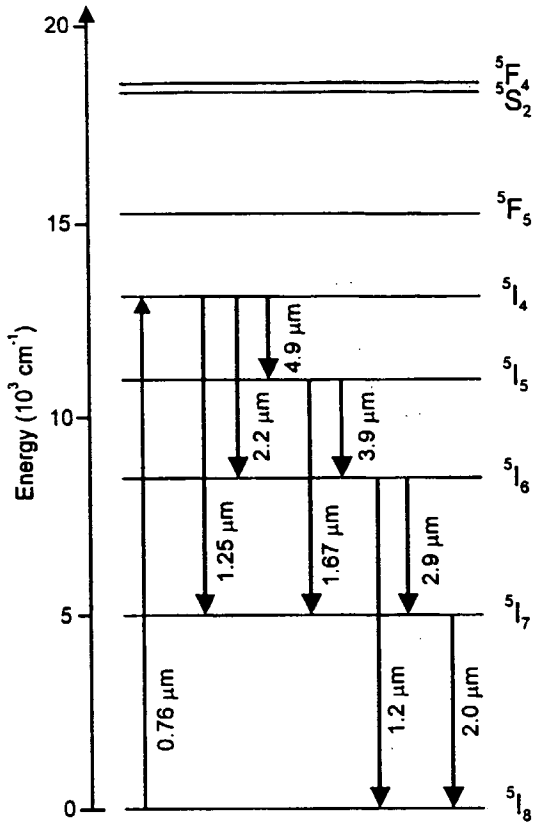
20
15
10
5
0
Energy (10^3 cm^{-1})
$^5F_4$
$^5S_2$
$^5F_5$
$^5I_4$
$^5I_5$
$^5I_6$
$^5I_7$
$^5I_8$
4.9 µm
2.2 µm
3.9 µm
1.25 µm
1.67 µm
2.9 µm
0.76 µm
1.2 µm
2.0 µm

Figure 3

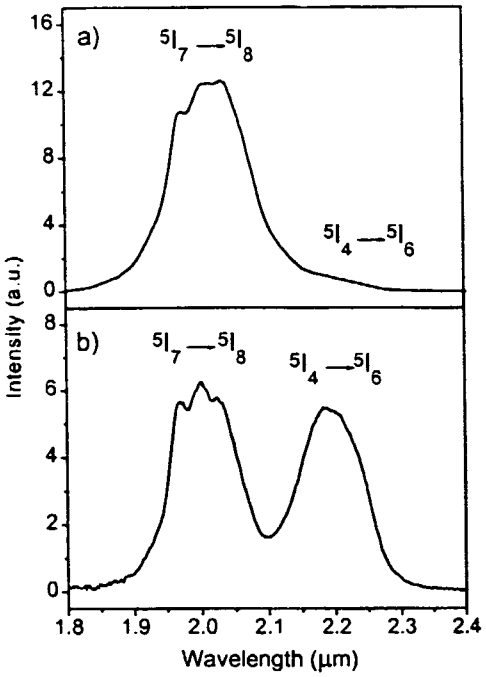
a)
$^5I_7 \rightarrow {}^5I_8$
$^5I_4 \rightarrow {}^5I_6$
b)
$^5I_7 \rightarrow {}^5I_8$
$^5I_4 \rightarrow {}^5I_6$
Intensity (a.u.)
Wavelength (μm)
16
12
8
4
0
8
6
4
2
0
1.8
1.9
2.0
2.1
2.2
2.3
2.4

Figure 4

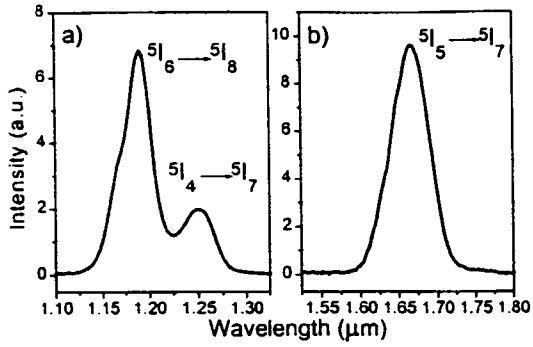
a)
$^5I_6 \rightarrow {}^5I_8$
$^5I_4 \rightarrow {}^5I_7$
b)
$^5I_5 \rightarrow {}^5I_7$
Intensity (a.u.)
Wavelength (μm)
0
2
4
6
8
10
1.10 1.15 1.20 1.25 1.30
1.55 1.60 1.65 1.70 1.75 1.80

Figure 5

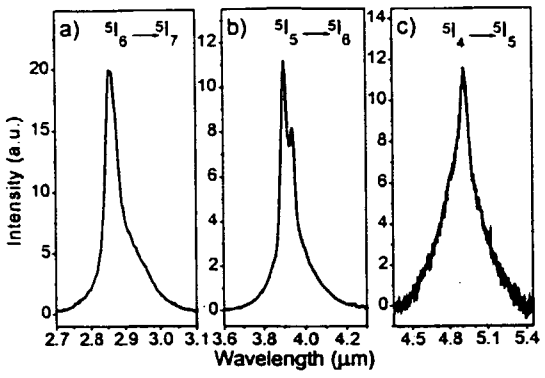
a) $^5I_6 \rightarrow {}^5I_7$
b) $^5I_5 \rightarrow {}^5I_6$
c) $^5I_4 \rightarrow {}^5I_5$
Intensity (a.u.)
Wavelength (μm)
2.7 2.8 2.9 3.0 3.1
3.6 3.8 4.0 4.2
4.5 4.8 5.1 5.4